Characterization of Human Saposins by NMR Spectroscopy†

Michael John,‡ Michaela Wendeler,§ Markus Heller,‡ Konrad Sandhoff,§ and Horst Kessler*,‡

Department Chemie, Technische Universität München, Lichtenbergstrasse 4, D-85747 Garching, Germany, and Kekulé-Institut für Organische Chemie, Universität Bonn, Gerhard-Domagk-Strasse 1, D-53121 Bonn, Germany

Received September 27, 2005; Revised Manuscript Received February 28, 2006

ABSTRACT: Saposins are lipid-binding and membrane-perturbing glycoproteins of the mammalian lysosomes involved in sphingolipid and membrane digestion. Although the four human saposins (Saps), A−D, are sequence-related, they are responsible for the activation of different steps in the cascade of lysosomal glycosphingolipid degradation. Saposin activity is maximal under acidic conditions, and the pH dependence of lipid and membrane binding has been assigned to conformational variability. We have employed solution NMR spectroscopy to all four ^{15}N-labeled human saposins at both neutral and acidic pH. Using backbone NOEs and residual dipolar couplings, the "saposin fold" comprising five α-helices was confirmed for Sap-A, Sap-C, and Sap-D. Structural variations within these proteins are in the order of variations between the known structures of Sap-C and NK-lysin. In contrast, Sap-B yielded spectra of very poor quality, presumably due to conformational heterogeneity and molecular association. Sap-D exists in a slow dynamic equilibrium of two conformational states with yet unknown function. At pH 4.0, where all saposins are highly unstable, Sap-C undergoes a transition to a specific dimeric state, which is likely to resemble the structure recently found in both Sap-C in a detergent environment and crystals of Sap-B.

Saposins ("sphingolipid activator proteins" or Saps)[1] are ∼10 kDa glycoproteins that are essential cofactors for the lysosomal in vivo degradation of glycosphingolipids with short oligosaccharide headgroups (*1*, *2*). Their sequences are up to 40% identical (up to 60% if considering amino acids with similar properties), including six strictly conserved cysteine residues with identical connectivity (*3*, *4*) and a common glycosylation site. However, the specificity and mode of activation among the four individual saposins, A−D, seem to differ considerably. For example, Sap-B stimulates the hydrolysis of the sulfate group from sulfatide by arylsulfatase A, whereas Sap-C is required for the degradation of glucosylceramide to ceramide (*5*). In contrast, Sap-D has been shown to accelerate sphingomyelinase activity (*6*) and is needed for the catabolism of glycosphingolipids containing α-hydroxylated acyl chains (*7*). A functional defect due to mutation in either saposin results in a specific phenotype of pathological storage of glycosphingolipids (*8*). Recently, the first patient with Sap-A deficiency was described (*9*), and that phenotype confirmed the findings from a Sap-A-deficient mouse line (*10*) that this saposin is indispensable for galactosylceramide catabolism.

Apart from their role in lysosomal sphingolipid degradation, other vital functions of the saposins are now beginning to emerge. Recent studies of a mouse model of complete Sap deficiency indicated that the saposins are essential for the biogenesis of the epidermal water permeability barrier (*11*−*13*). Furthermore, it has recently been demonstrated that the saposins are crucially involved in the presentation of lipid antigens by CD1 molecules (*14*, *15*). Sap-D has been reported to solubilize anionic phospholipid-containing membranes, (*16*) whereas Sap-C induces phospholipid vesicle fusion (*17*, *18*) and membrane restructuring (*19*, *20*).

The saposin motif occurs not only in sequence-related homologues from different functional families but also as a subsequence of larger proteins (*21*, *22*). The three-dimensional fold of these saposin-like proteins ("SapLIPs") and domains has been revealed by the solution structure of porcine NK-lysin, an unglycosylated effector polypeptide of T-cells and natural killer (NK) cells (*23*). It is formed from five α-helices: a long helix α1, against which helices α2 and α3 are packed from one side, and helices α4 and α5 from the other side. This relatively compact fold has also been seen in the recently published solution structure of Sap-C (*24*). Although both proteins possess membrane binding capability, their surface electrostatic potential is remarkably different, being highly negative for Sap-C (pI 4.5) and mostly positive for NK-lysin (pI 9.2).

A different fold into a homodimeric structure made up of two V-shaped monomers, which form a shell around a large hydrophobic cavity, was observed in the crystal structure of Sap-B (*25*). Although the secondary structure is similar to that of the known monomeric members of the saposin family, the tertiary arrangement of helices is remarkably different, with helices α2 and α3 being turned far away from α1. In contrast, helices α3 and α4, which are nearly orthogonal to

† This work was supported by the Deutsche Forschungsgemeinschaft and the Fonds der chemischen Industrie.

* To whom correspondence should be addressed. Telephone: ++49-89-289-13300. Fax: ++49-89-289-13275. E-mail: horst.kessler@ch.tum.de.

‡ Technische Universität München.

§ Universität Bonn.

[1] Abbreviations: Sap, sphingolipid activator protein; NMR, nuclear magnetic resonance; NK, natural killer; HSQC, heteronuclear single-quantum coherence; GM, ganglioside molecule; NOESY, nuclear Overhauser enhancement spectroscopy; TOCSY, total correlation spectroscopy; DMPC, dimyristoylphosphatidylcholine; DHPC, dihexanoylphosphatidylcholine; SDS, sodium dodecyl sulfate; RDC, residual dipolar coupling; PDB, Protein Data Bank.

10.1021/bi051944+ CCC: $33.50 © 2006 American Chemical Society
Published on Web 03/30/2006

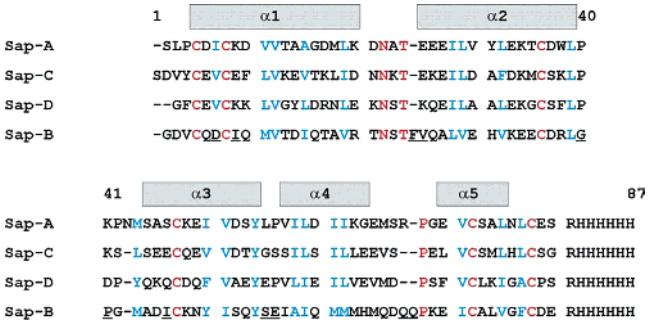

FIGURE 1: Sequences of human saposins used in this study. To facilitate comparisons between the proteins, residues are numbered according to the sequence of Sap-C. The alignment, which was generated with CLUSTALX (*31*), assigns insertions of an asparagine after Pro[42] and an arginine after Ser[67] to Sap-A, as well as an insertion of a phenylalanine (after Thr[24]) and two glutamate residues after Asp[67] to Sap-B. Strictly conserved cysteines and other hydrophilic residues are colored red, whereas conserved hydrophobic residues are colored blue. Five helices, α1−α5, are indicated above the sequence, and the sequence motifs unique to Sap-B are underlined.

each other in the monomer, are separated by only a minor tilt in the dimer. A similar fold has been found for Sap-C in a detergent environment (*26*).

To explain the strong pH dependence of saposin activity and their lipid and membrane binding properties, it has been proposed that the saposins possess inherent conformational variability (*27*, *28*). This feature is significant as none of the above-mentioned structures has been explicitly determined under typical lysosomal acidic conditions at which activity is maximal. Furthermore, helix repacking in the Sap-B dimer has raised the question of whether the specificity of the remaining two saposins, Sap-A and Sap-D, for which no structural data are available, is the result of similar conformational variances. The physiological function and mode of action of both Sap-A and Sap-D are yet poorly understood.

Recently, we demonstrated that the human GM2 activator can be labeled with ^{15}N for NMR with high efficiency in the methylotropic yeast *Pichia pastoris* (*29*). It turned out that this expression system was also applicable to the human saposins A−D with the sequences shown in Figure 1 and yielded large amounts of homogeneous and unglycosylated proteins. It has been shown that the absence of glycosylation has no significant effect on the stability and activity of the saposins (*4*, *30*). Here we report on a study of all four ^{15}N-labeled human saposins by solution NMR spectroscopy at both acidic (pH 4.0) and neutral pH (pH 7.0).

MATERIALS AND METHODS

Protein Expression and Purification. The sequences of saposins A−D (Figure 1) were furnished with a C-terminal Arg-$(His)_6$ tag and expressed in *P. pastoris* (strain GS115) using the pPIC9K expression vector and a modified FM22 medium (*32*) as described for the GM2 activator (*29*). Briefly, 200 mL of FM22-Gluc [containing KH_2PO_4, $(^{15}NH_4)_2SO_4$ (Cambridge Isotope Laboratories, Andover, MA), $CaSO_4$, K_2SO_4, $MgSO_4$, biotin, PTM1, and 1% (w/v) glucose] were inoculated with a 15 mL overnight culture of a *P. pastoris* transformant and grown at 30 °C and pH 4.9 to an OD_{600} of 3−6. Cells were harvested by centrifugation, resuspended in 500 mL of FM22-Met medium [containing 0.5% (v/v) methanol instead of glucose] and incubated for a further 76 h at 30 °C, with additional methanol supplied every 24 h. From the supernatant, the respective recombinant protein was purified by NiNTA chromatography (Qiagen, Hilden, Germany) followed by gel filtration on a Superdex 75 column (HiLoad 16/60 prep grade, Amersham-Pharmacia Biotech, Uppsala, Sweden). Fractions containing purified saposins were combined and concentrated to approximately 1.2 mM in 50 mM acetate (pH 4.0) or phosphate (pH 7.0) buffer containing 100 mM NaCl. Protein homogeneity and isotopic labeling (>98%) were confirmed by ESI-TOF mass spectrometry on a Q-TOF 2 mass spectrometer (Micromass, Manchester, U.K.). The samples were transferred to Shigemi NMR tubes (Shigemi Ltd., Tokyo, Japan), and 5% (v/v) D_2O was added.

^{15}N HSQC Spectra and Diffusion Measurements. NMR experiments were performed on Bruker (Bruker Biospin, Rheinstetten, Germany) spectrometers equipped with TXI gradient probes and, unless stated otherwise, at a proton frequency of 600 MHz. All spectra were processed with XWINNMR (Bruker Biospin) and analyzed with SPARKY (T. D. Goddard and D. G. Kneller, University of California, San Francisco, CA). ^{15}N HSQC spectra were recorded with eight transients and a time domain size of 128 × 512 complex data points in approximately 40 min, corresponding to acquisition times of 100 and 86 ms for the ^{15}N and $^1H^N$ dimensions, respectively. For each sample, the temperature was varied in steps of 10 °C from 17 to 57 °C, and spectra were referenced externally to 3-(methylsilyl)propionic acid dissolved in the same buffers. NMR diffusion measurements were performed for Sap-B and Sap-C at pH 7.0 and 37 °C using bipolar pulse gradients (*33*) with a maximum strength of 54 G/cm and a diffusion delay of 150 ms. Gradient strengths were calibrated assuming a proton diffusion coefficient of 3.3×10^9 m^2 s^{-1} of a pure water sample and using a diffusion delay of 25 ms.

Resonance Assignments and Secondary Structure. For Sap-A, Sap-C, and Sap-D at pH 7.0 and Sap-C at pH 4.0, a set of four ^{15}N-edited three-dimensional spectra was recorded: NOESY-^{15}N HSQC (*34*), ^{15}N HSQC-NOESY-^{15}N HSQC (*35*), TOCSY-^{15}N HSQC (*36*), and HNHB (*37*). Each experiment was acquired with eight transients and a time domain size of 96 × 36 (^{15}N) × 512 ($^1H^N$) complex data points, which required approximately 1.5 days. Mixing periods were 120 ms for NOESY and 80 ms for the TOCSY experiment. For TOCSY mixing, a clean-CITY sequence (*38*) was used. Sequential connectivities were established using the strong helical $d_{NN}(i, i + 1)$ NOE. The TOCSY-^{15}N HSQC and HNHB spectra provided the resonance frequencies of H^α, H^β, and further side chain protons required for the amino acid identification. For the pH 7.0 samples, all spectra were acquired at 37 °C, except for those of Sap-D, where a second data set was recorded at 17 °C to resolve ambiguities resulting from signal overlap. For the monomeric and dimeric forms of Sap-C at pH 4.0, resonance assignments were carried out at 17 and 57 °C, respectively, and transferred to 37 °C. Additional high-resolution NOESY-^{15}N HSQC spectra [256 × 24 (^{15}N) × 1024 ($^1H^N$) complex data points, 2.5 days each] were recorded for Sap-A, Sap-C, and Sap-D on a 900 MHz spectrometer.

Residual Dipolar Couplings. Bicellar solutions (15%, w/v) were prepared according to a standard procedure with a 3:1:

0.1 DMPC:DHPC:SDS molar ratio. The stock solution of Pf1 bacteriophage (52 ± 4 mg/mL) was purchased from ASLA (ASLA Biotech Ltd., Riga, Latvia) and used without further purification. The cold stock was added to 300 μL of the phosphate-buffered 1.2 mM solutions (pH 7.0) of Sap-A, Sap-C, and Sap-D, until the largest $N-H^N$ dipolar couplings reached ~20 Hz. This was the case at 100 μL (corresponding to 13 mg/mL) for Sap-C and Sap-D and 300 μL (26 mg/mL) for Sap-A. IPAP-[^{1}H,^{15}N]-HSQC spectra (*39*) of aligned and reference samples were recorded at 37 °C on a 750 MHz spectrometer with a time domain size of 256 × 512 complex data points, corresponding to a ^{15}N acquisition period of 160 ms ($\sim T_2$). The data matrix was further linear predicted to a size of 384 × 512 and zero-filled to 1024 × 1024 (~0.7 Hz digitization) prior to Fourier transformation. Peaks were fitted to a Gaussian line shape, and a uniform uncertainty of the final dipolar couplings of 1 Hz was assumed. Computational homology models were obtained from the SWISS-MODEL server (*40*) using the sequence alignment of Figure 1 and the experimental structures of the homodimeric Sap-B (PDB entry 1N69, chain C), Sap-C (PDB entry 1M12), and NK-lysin (PDB entry 1NKL) as templates. For fitting of RDC data to these models, MODULE (*41*) was used. The errors of the fit parameters were estimated by repeating the fit with 100 data sets created by random exclusion of up to three data points.

Exchange Rates in Sap-D. Exchange rates in Sap-D were measured at 17, 27, 37, 47, and 57 °C on a 600 MHz spectrometer equipped with a cryogenic probe, using two-dimensional heteronuclear exchange spectroscopy (*42*). For each of the 10 mixing periods (8, 32, 62, 122, 182, 272, 362, 482, 602, and 722 ms), a data matrix of 96 × 512 complex points was recorded in approximately 2 h. A long recycle delay of 4 s ensured fully relaxed conditions at the beginning of each transient. The intensities of the two "auto" (=^{15}N HSQC) and two "exchange" peaks of residue Cys^{36} were fitted with a MATLAB (MathWorks Inc., Natick, MA) code to a two-site model with two equilibrium polarizations and a forward and backward exchange rate. Identical ^{15}N line widths, ^{15}N longitudinal relaxation during mixing, and ^{1}H transverse relaxation during the INEPT periods were assumed for both conformers.

RESULTS

^{15}N HSQC Spectra at Neutral pH. We first recorded ^{15}N HSQC spectra of all saposins at variable temperatures in phosphate buffer at pH 7.0. These samples shared a remarkable thermal robustness, and no change in the spectra could be observed after heating to 57 °C or long-term storage. Above 37 °C, however, signals began to disappear due to fast solvent exchange of amide protons. Peak positions and line widths were independent of the protein concentration over the 0.5−2 mM range, indicating a weak tendency to form unspecific aggregates, as expected for highly acidic proteins (pI <5). Only when Sap-C was further concentrated to 4 mM did the peaks started to broaden substantially. ^{15}N HSQC spectra of the four proteins at 37 °C are compared in Figure 2.

Clearly, Sap-C yields the most appealing $N-H^N$ correlation map (Figure 2C). Although the peaks show the limited frequency dispersion of α-helical proteins (<15 ppm in the ^{15}N dimension and <2 ppm in the $^1H^N$ dimension), almost all of them are resolved at 37 °C, with line widths typical of a monomeric and conformationally homogeneous protein. This spectrum is nearly identical with a recently published spectrum of Sap-C recorded under similar experimental conditions (*24*). Spectra of reasonable quality were also obtained for Sap-A and Sap-D; these proteins, however, show signs of inherent conformational heterogeneity: Sap-D exists in two distinct conformations yielding two separate sets of resonances with relative intensities of approximately 2:1 (Figure 2D). In Sap-A (Figure 2A), the resonance line widths and intensities are not uniform and depend on the temperature and magnetic field strength, indicating that this protein is subject to conformational exchange processes at the intermediate time scale. For all three proteins, average ^{15}N longitudinal and transverse relaxation rates yielded molecular correlation times (τ_c) of 4−4.5 ns, i.e., monomeric species.

Table 1: Human Saposins A−D in Solution

protein	pH 4.0[a]	pH 7.0[a]
Sap-A	strongly aggregated	monomeric, multiple conformations (69/78)
Sap-B	dimeric, multiple conformations	dimeric, multiple conformations
Sap-C	monomeric (77/78) > 27° dimeric (68/78)	monomeric (72/78)
Sap-D	monomeric, two conformations	monomeric, two conformations (70/77)

[a] The numbers in parantheses specify the fraction of non-proline residues (excluding the hexahistidine tag) with assigned ^{15}N, $^1H^N$, and $^1H^\alpha$ resonances.

In contrast, the ^{15}N HSQC spectra of Sap-B recorded under the same conditions are of very poor quality, which could not be substantially improved by varying the temperature, protein concentration, and magnetic field (Figure 2B). In addition, ^{15}N transverse relaxation rates seem strongly non-uniform and affected by exchange broadening, thereby preventing a determination of τ_c and thus the molecular association state. To circumvent this problem, we measured the protein's translational diffusion coefficient (D_t) and found a value of (1.58 ± 0.06) × 10^{-10} m^2/s, compared with a value of (1.97 ± 0.04) × 10^{-10} m^2/s for the monomeric Sap-C. The smaller value obtained for Sap-B is in agreement with a dimeric species or a nonspecific mixture of higher association states with the average being a dimer. The behavior of all four saposins in solution is summarized in Table 1.

For the "well-behaved" proteins Sap-A, Sap-C, and Sap-D, we were able to use the strong sequential $d_{NN}(i, i+1)$ NOE correlations to assign the ^{15}N HSQC peaks of residues within the helices. Most of the remaining nonhelical residues were assigned via intermediate-range correlations, except for a small number of residues which could not be assigned due to fast solvent exchange of their amide protons or overlap. This procedure was substantially more complex in the case of Sap-D, since both NOESY and TOCSY spectra contained additional exchange and exchange-relayed correlations due to an equilibration between the two conformers during the mixing periods (see below). All further data of Sap-D described in the following refer to the major conformer.

The typical helical d_{NN} and $d_{\alpha N}$ NOE patterns and H^α secondary chemical shifts confirmed that in all three proteins the helices span the identical sequence positions: 5−20 (α1),

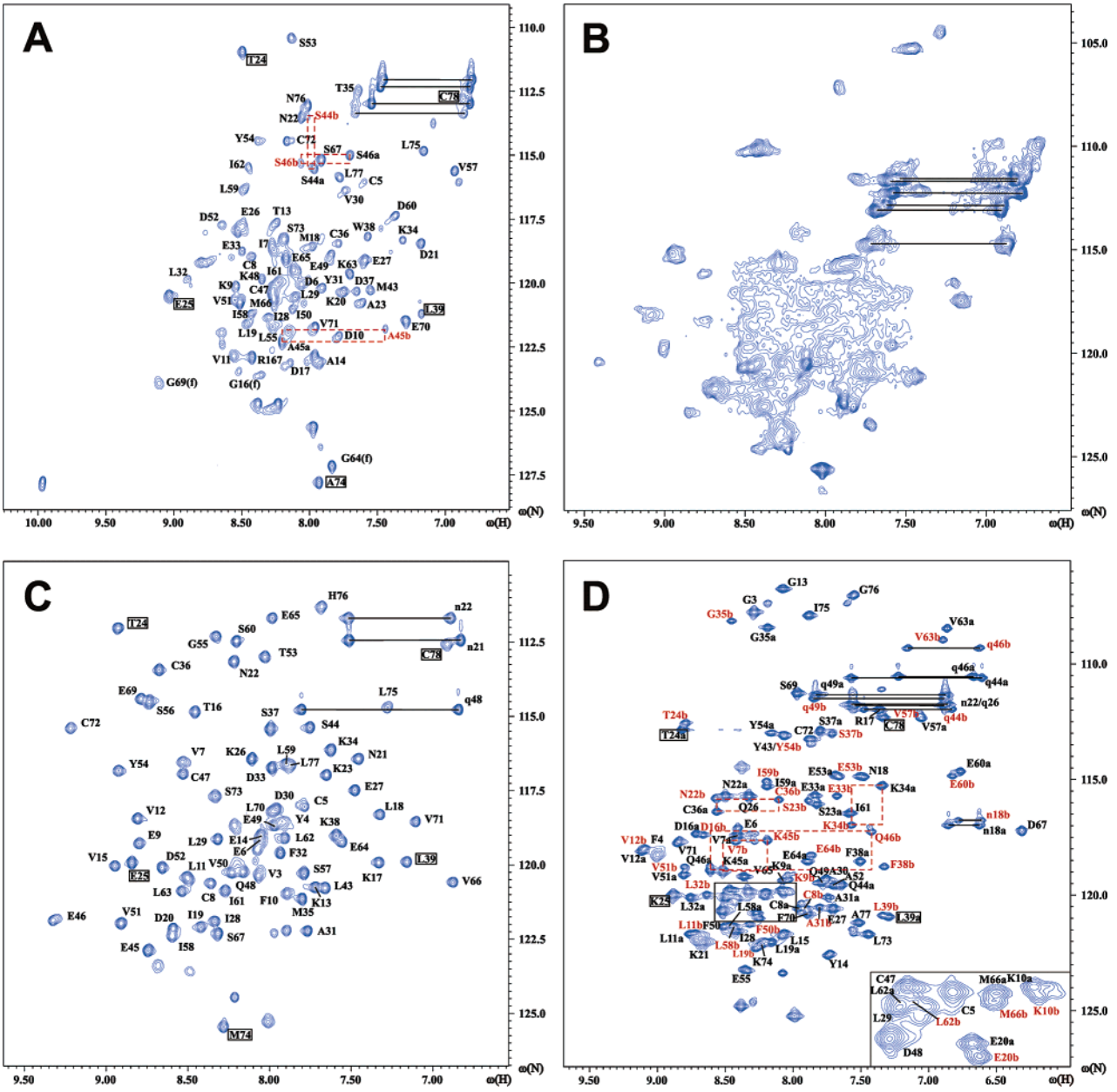

FIGURE 2: ^{15}N HSQC spectra of saposins A−D (A−D), recorded on a 600 MHz spectrometer at pH 7.0 and 37 °C. Assigned resonances are labeled with the residue name and, if appropriate, additionally with a (black) and b (red) for the major and minor conformers, respectively. Large frequency separations between both conformers are highlighted with red dashed rectangles, whereas conserved residues 24, 25, 39, 74, and 78 (see the text) are highlighted with black boxes. Side chain NH_2 groups are indicated by horizontal lines and labeled with lowercase letters. The most crowded region in spectrum D is expanded in the bottom right corner.

25−39 (α2), 44−54 (α3), 57−64 (α4), and 69−75 (α5). Furthermore, most of the NOE correlations that were crucial for assigning the three loop regions (α1−α2, α3−α4, and α4−α5) turned out to be conserved, whereas the α2−α3 loop remained unassigned. Strong similarities between the assigned ^{15}N HSQC spectra of Sap-A, Sap-C, and Sap-D indicate that many amide groups experience identical environments. For example, the highly conserved residues Thr^{24} and Cys^{78} always appear in the top left and right corners, respectively, and Leu^{39} always belongs to the residues with the lowest $^{1}H^{N}$ frequencies. Even many nonconserved residues are found at similar positions, such as Glu^{25} in Sap-A and Sap-C and Lys^{25} in Sap-D, or Met^{74} in Sap-C and Ala^{74} in Sap-A (Figure 2).

Residual Dipolar Couplings. In contrast to the wealth of sequential and intrahelical NOEs, the recorded NOESY spectra did not yield sufficient unambiguous interhelical NOE data for a determination of the three-dimensional fold of Sap-A and Sap-D. However, a few long-range correlations across the expected Cys^{5}−Cys^{78} and Cys^{8}−Cys^{72} disulfide bonds confirmed that the disulfide bond pattern in these proteins is conserved. We therefore decided to measure $N-H^{N}$ residual dipolar couplings (RDCs), which yield information about the orientation of $N-H^{N}$ bond vectors and therefore the helical axes. As alignment media, we chose phospholipid bicelles (*43*) and Pf1 bacteriophage (*44*).

Remarkably, in 5% (w/v) bicellar solutions, the splitting of the ^{2}H resonance instantaneously collapsed after the addition of only 40 μM Sap-C, even if the bicelles were prepared with SDS to enhance electrostatic repulsion. At lower protein concentrations, some alignment was retained, but the phase turned out to be not stable over the longer

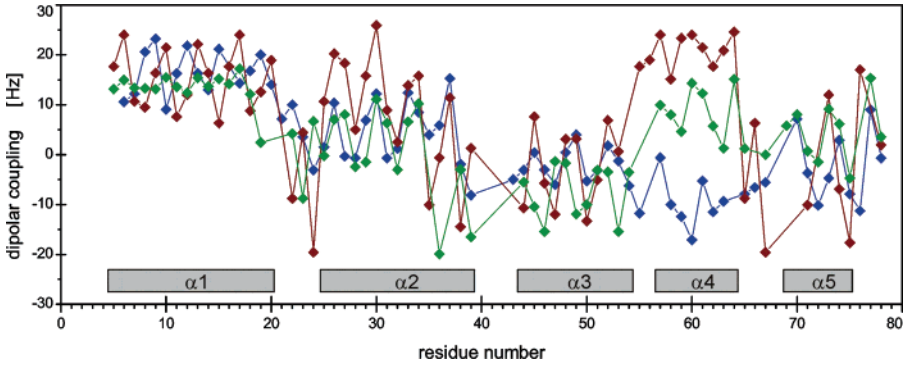

FIGURE 3: $N-H^N$ residual dipolar couplings in Sap-A (blue), Sap-C (red), and Sap-D (green) obtained from alignment with Pf1 bacteriophage. The data points are connected with solid lines, and missing data are due to fast hydrogen exchange or signal overlap. Helices α1−α5 are represented with gray bars.

time period required for protein spectra under these conditions. We find this behavior worth mentioning as, in contrast to previous results (*24*), it indicates some interaction between Sap-C and the lipids at neutral pH, thereby preventing the latter from forming a stable liquid crystalline phase. This phenomenon was not investigated further for the other saposins or at low pH where protein−lipid interactions are expected to increase in strength.

The alignment of Sap-A, Sap-C, and Sap-D at pH 7.0 using Pf1 bacteriophage was straightforward and required 13 mg/mL (for both Sap-C and Sap-D) and 26 mg/mL Pf1 phage (for Sap-A). Although the resulting solutions were macroscopically highly viscous, the average rate of ^{15}N transverse relaxation (R_2) increased only slightly from 7.4 s^{-1} to 8.5 s^{-1} in the presence of 26 mg/mL phage. No substantial changes were observed in the ^{15}N HSQC spectra, confirming that the structures of the proteins remain intact.

Figure 3 shows a plot of the experimental dipolar couplings of Sap-A, Sap-C, and the major conformer of Sap-D versus the residue number. In each of helices α1−α5, the values describe a characteristic oscillating pattern, which has recently been termed a "dipolar wave" (*45*) and arises from the fact that helical $N-H^N$ bond vectors are generally not oriented perfectly parallel but rather are located on a cone with an opening angle of approximately 16°. The average value within a given helix depends on both the orientation of the helix axis with respect to the molecular frame and the alignment of this molecular frame with respect to the external magnetic field, the latter being described by the alignment tensor. The patterns observed for Sap-A, Sap-C, and Sap-D are highly similar, except for helix α4, where a large difference in the average couplings suggests that this helix may be oriented differently in the three proteins.

Notably, the couplings obtained for Sap-C also do not perfectly correlate with previously published data (*24*), although the experimental conditions are very similar (pH 7.0 vs pH 6.8, 37 °C vs 25 °C, 0.9 mM vs 0.8 mM, and 13 mg/mL Pf1 phage vs 15 mg/mL Pf1 phage). Both data sets could be fitted equally well to the structure of Sap-C, but the orientation and rhombicity of the resulting alignment tensors were substantially different (Table 2). We explain this via the presence of a hexahistidine tag in our protein preparation, a large positively charged patch that can significantly modulate the electrostatic interaction with the highly negatively charged surface of the Pf1 coat protein (*46*). For the same reason, the alignment tensors of Sap-A and Sap-D are expected to differ from the tensor of Sap-C due to nonconservation of charged residues (*47*).

Table 2: Alignment of Sap-A, Sap-C, and Sap-D in Pf1 Filamentous Phage

protein	[Pf1] (mg/mL)	D_{ax} (Hz)[a]	R[a]	α (deg)[b]	β (deg)[b]	γ (deg)[b]
Sap-A	26	11.7 ± 0.8	0.58 ± 0.04	58 ± 4	155 ± 2	51 ± 3
Sap-C	13	15.1 ± 0.4	0.50 ± 0.02	35 ± 2	166 ± 1	61 ± 2
Sap-C[c]	15	23.0 ± 0.3	0.31 ± 0.02	6 ± 1	164 ± 0	42 ± 1
Sap-D	13	11.3 ± 1.0	0.36 ± 0.04	66 ± 6	171 ± 1	55 ± 4

[a] The tensors were obtained by fitting the dipolar couplings to the equation $D_{NH} = D_{ax}(3\cos^2\theta - 1 + R\sin^2\theta\cos 2\phi)$, where θ and ϕ denote the $N-H^N$ bond vector orientations of the Sap-C structure (PDB entry 1M12) with respect to the tensor frame. For Sap-A and Sap-D, the tensors were determined using protein models generated from the Sap-C structure. [b] The Euler angles correspond to successive rotations around the *zxz* axes. [c] Data from ref *24*.

For Sap-A and Sap-D, we generated model structures using both the solution structure of Sap-C (PDB entry 1M12) (*24*) and chain C of the crystal structure of Sap-B (PDB entry 1N69) (*25*). These models are strongly biased toward the respective template; for example, the 1M12 models of Sap-A and Sap-D can be superimposed onto Sap-C with a backbone rmsd of 0.7 Å for all residues. We then fitted the measured dipolar couplings to these models, with the results shown in Figure 4.

Clearly, the correlation is much stronger for the 1M12 models (Figure 4A,B) than for the 1N69 models (Figure 4D,E), suggesting that in solution both Sap-A and Sap-D adopt a fold which resembles much more Sap-C than Sap-B. The strongest outliers (>7 Hz) arising from the 1M12 model of Sap-D (Figure 4B) are located either at the N-terminus (Gly^3 and Phe^4), in loop regions (Glu^{20}, Lys^{21}, Glu^{55}, Met^{66}, and Gly^{76}), or in helix α2 (Gly^{35} and Ser^{37}). In contrast, for the respective 1N69 model (Figure 4E), we did not find such a correlation with sequence. The results are analogous for Sap-A, except that different residues (Ala^{23}, Val^{30}, Lys^{34}, Thr^{35}, Cys^{36}, Met^{43}, Glu^{65}, and Ser^{73}) deviate for the 1M12 model (Figure 4A). Notably, helix α2 is also a source of deviations if the measured couplings of Sap-C are fitted against the published structure itself (Figure 4C). For comparison, we fitted the Sap-C data to a model built from the solution structure of NK-lysin (PDB entry 1NKL) and obtained a correlation which is comparable to a fit of the Sap-A and Sap-D data to the structure of Sap-C (Figure 4F). These results suggest that the four proteins (Sap-A, Sap-C, Sap-D, and NK-lysin) share a highly similar fold, whereas

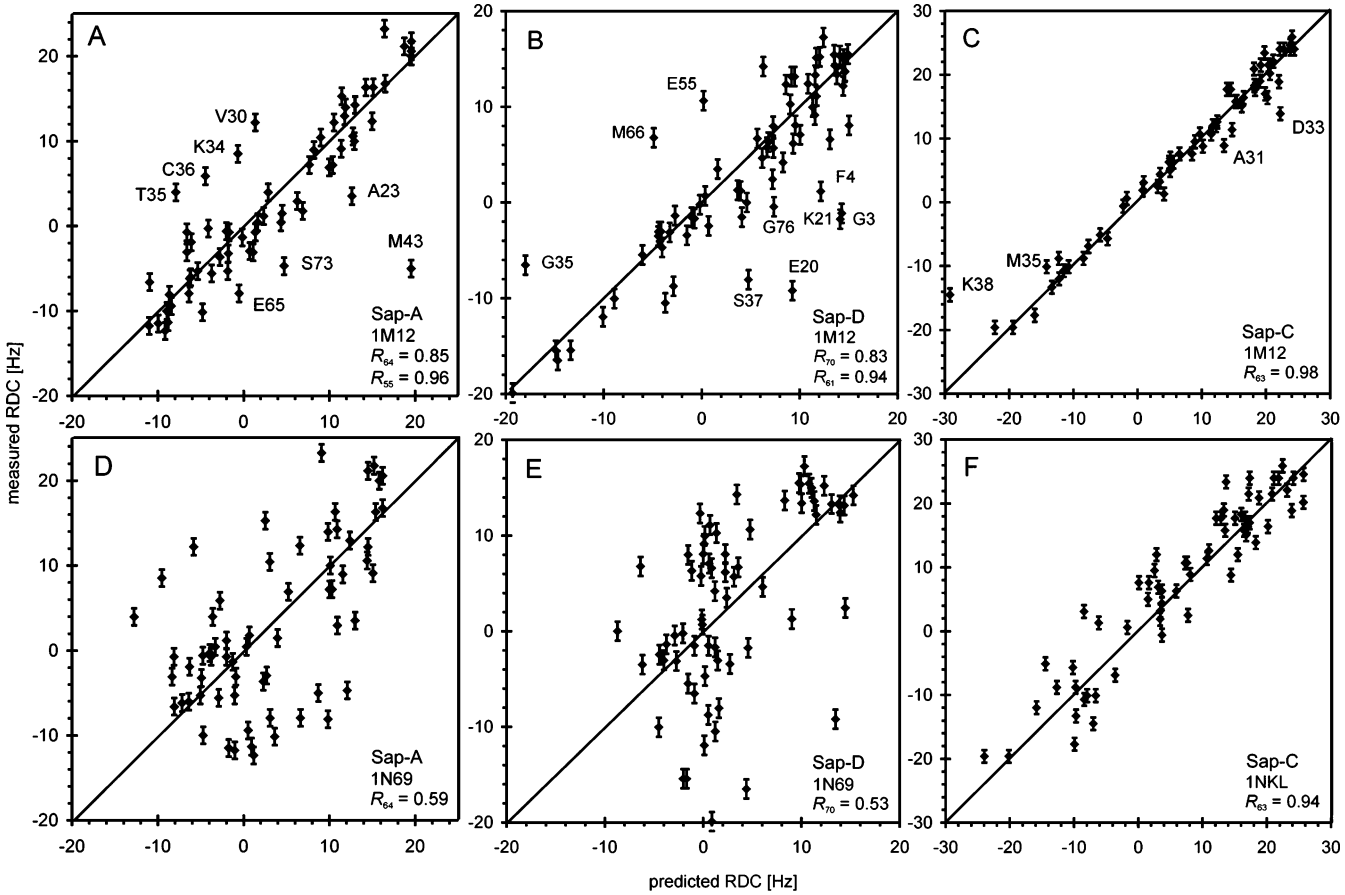

FIGURE 4: Correlation of measured dipolar couplings of Sap-A, Sap-C, and Sap-D vs values back-calculated using different model structures. (A−C) Data of Sap-A, Sap-D, and Sap-C against the solution structure of Sap-C (PDB entry 1M12). Outliers with a >7 Hz (for C, 5 Hz) deviation are labeled. (D and E) Data of Sap-A and Sap-D against chain C of the crystal structure of Sap-B (PDB entry 1N69). (F) Data of Sap-C against the solution structure of NK-lysin (PDB entry 1NKL). The Pearson coefficients R_N are indicated, where N is the number of couplings used in the fit.

the open conformation adopted in the Sap-B dimer seems to be unique under neutral-pH conditions.

To validate the significance of the observed differences between these correlations, we created 100 data sets for each protein by random exclusion of up to three experimental couplings and repeated the fitting against the models. This procedure not only yielded error estimates for the tensor parameters presented in Table 2 but also strongly supported the 1M12 models for Sap-A and Sap-D. Whereas the fitted tensors obtained from the 1M12 models of Sap-A and Sap-D are very robust against random exclusions, much larger variations are observed for the 1N69 models (data not shown). Notably, the correlations for Sap-A and Sap-D are not substantially improved if all couplings from α4 are excluded from fitting. This indicates that the deviations between observed and calculated couplings are likely to be due to local structural fluctuations among Sap-A, Sap-C, and Sap-D rather than different helical orientations, and the variations in the couplings between the proteins are due to their different alignment in solution. Table 2 shows that the alignment tensors obtained for the three proteins are significantly tilted with respect to each other and also strongly vary in their rhombicity.

Conformational Exchange in Sap-D. As mentioned above, spectra of Sap-D recorded at pH 7.0 revealed the existence of two distinct conformations in a ratio of approximately 2:1. Both conformers undergo considerable exchange at 37 °C during the mixing periods of NOESY and TOCSY spectra, making resonance assignment at this temperature more challenging than for the other saposins. To further complete the assignment, we repeated the experiments at 17 °C where exchange is slowed and almost invisible. ^{15}N HSQC spectra of Sap-D recorded at pH 4.0 exhibited a similar 2:1 equilibrium, although the limited stability of the protein under these conditions did not permit the resonance assignment.

The assigned ^{15}N HSQC spectrum recorded at pH 7.0 (Figure 2D) shows that for most residues the peaks belonging to the major (a) and minor (b) conformers are very close or even merged, indicating they experience almost the same chemical environment. Large frequency separations occur in only the two stretches, Lys^{34}−Cys^{36} (helix α2) and Lys^{45}−Gln^{46} (helix α3), which are linked by the Cys^{36}−Cys^{47} disulfide bond. In contrast, the sequentially neighboring residues Ser^{37}−Leu^{39} and Tyr^{43}−Gln^{44}, which further extend to the α2−α3 loop, are much less affected. Notably, we observed a similar frequency-separated second set of peaks for Ser^{44}−Ser^{46} of Sap-A (Figure 2A). For all of these residues, we carefully analyzed the sequential d_{NN} and $d_{\alpha N}$ NOE pattern and found no evidence for a different backbone conformation. Likewise, the N−H^N dipolar couplings observed for both conformers of Sap-D are identical within experimental error, except for Cys^{36} and Ser^{37}, where they deviate by ∼5 Hz.

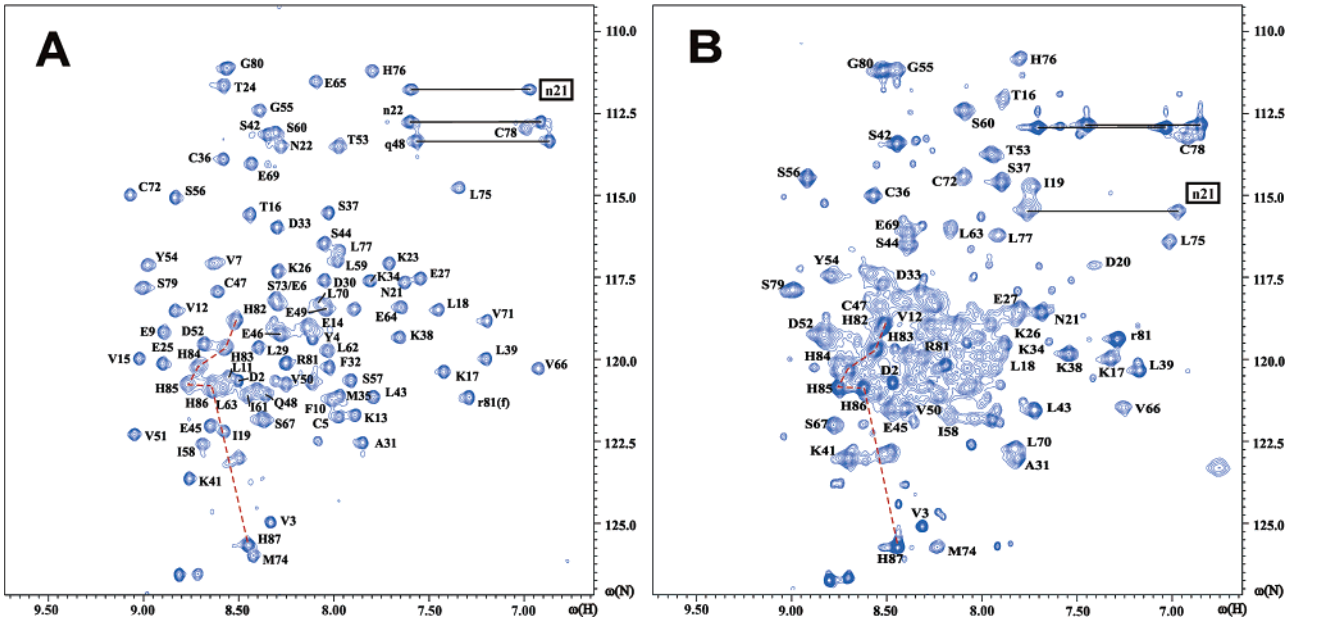

FIGURE 5: ^{15}N HSQC spectra of a 1.2 mM sample of Sap-C at pH 4.0 (A) recorded after 0.5 h and (B) recorded after 15 h at 37 °C on a 600 MHz spectrometer. Residue labeling corresponds to Figure 2. The signals belonging to the hexahistidine tag are connected with a red dashed line, whereas the side chain NH_2 group of Asn^{21} is highlighted with a black box.

Using two-dimensional heteronuclear exchange spectroscopy (*42*), we measured forward and backward exchange rates, k_a and k_b, between conformers a and b as a function of temperature and obtained the following activation energies: $\Delta E_a^{\ddagger} = 18.0 \pm 0.5$ kcal/mol and $\Delta E_b^{\ddagger} = 16.2 \pm 0.5$ kcal/mol, respectively. The temperature dependence of the equilibrium constant k_b/k_a, which is identical to the ratio of populations p_a/p_b observed in the ^{15}N HSQC spectra, yielded an equilibrium enthalpy ΔH of 1.8 ± 0.3 kcal/mol and an equilibrium entropy ΔS of 4.6 ± 0.8 cal mol^{-1} K^{-1}. This partial energetic compensation of both positive ΔH and ΔS corresponds to an order−disorder transition which is often found for kinetic data of biological systems (*48*), although this principle has been challenged recently (*49*).

An energetic barrier of 16−18 kcal/mol is typical of proline cis−trans isomerizations in a nonrigid environment (*50*). Two proline residues (Pro^{40} and Pro^{42}) are located in the α2−α3 loop of Sap-D, but we were unable to provide evidence of their isomerization due to a lack of assignment of the amide group of Asp^{41} and resonance overlap in Tyr^{43}. An isomerization of Pro^{40} seems unlikely, however, since the NOESY strips for Leu^{39}a and Leu^{39}b are highly similar. In this context, it should also be noted that Pro^{40} is conserved in Sap-C, where conformational exchange is completely absent, whereas Pro^{42} is conserved in only the two conformationally heterogeneous proteins, Sap-A and Sap-D.

Alternatively, the occurrence of two conformations of Sap-D with a high-energy barrier can be explained by an isomerization of the Cys^{36}−Cys^{47} disulfide bond geometry similar to what has been described for BPTI (*51*). Whereas for free cysteines in aqueous solution this process requires only very low activation energies (*52*), individual conformations can become distinguishable by NMR in proteins because of steric constraints imposed by rigid backbones. Such an isomerization would explain why the largest chemical shift changes occur in the sequential neighbors of Cys^{36} and Cys^{47} and without conformational changes in the backbone. However, the isomerization would require a substantial change in the χ_1 angle in one of the cysteines, which we can exclude for Cys^{36} ($\chi_1 \approx -60°$), but not for Cys^{47} due to overlap.

^{15}N HSQC Spectra at Acidic pH. To gain some insight into the pH dependence of saposin activity, we prepared samples of all proteins in acetate buffer at pH 4.0. All of these samples were highly unstable and typically degraded within a few days. Under these conditions, Sap-A is strongly prone to aggregation even at low concentrations and yielded ^{15}N HSQC spectra in which only the signals belonging to the hexahistidine tag were resolved. In contrast, spectra of fresh samples of the other saposins resembled the respective spectra obtained at pH 7.0. The 2:1 conformational equilibrium in Sap-D also exists at low pH, but the sample stability was not sufficient for resonance assignment even at 17 °C. Furthermore, the line widths were no longer independent of the protein concentration. For example, the apparent molecular correlation time of Sap-C increased by 30% if measured in a 2.1 mM solution compared to that in a 1.2 mM solution, indicating significant unspecific aggregation at higher protein concentrations.

The ^{15}N HSQC spectrum of a fresh 1.2 mM sample of Sap-C at pH 4.0 is shown in Figure 5A. Although the dispersion and certain patterns of peaks are similar to the spectrum recorded at pH 7.0 (Figure 2C), the individual resonances cannot be mutually correlated simply by overlaying the two spectra. However, we were able to reassign Sap-C at a lower temperature (17 °C) and observed an NOE pattern which was virtually indistinguishable from that obtained at pH 7.0. Large chemical shift differences of amide protons occur in residues which form hydrogen bonds to side chain carboxylates in the reported Sap-C structure, such as Cys^{5}, Thr^{24}, Glu^{46}, and Glu^{69}. In contrast, the resonance frequencies of H$^{\alpha}$ and other aliphatic protons, which are much less charge-sensitive, remain nearly invariant between pH 7.0 and 4.0. This confirms the previous suggestion that major conformational changes do not occur under acidic conditions

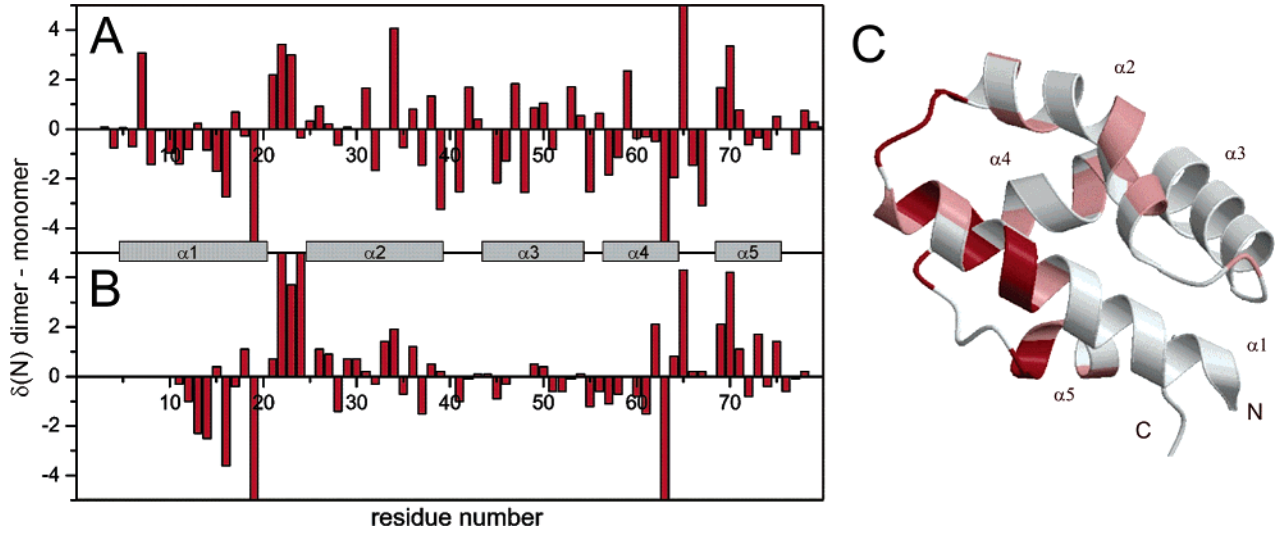

FIGURE 6: ^{15}N chemical shift changes in Sap-C induced by (A) the detergent SDS (*26*) and (B) dimerization at low pH. The values in panel B are mapped onto the structure of monomeric Sap-C in panel C: colorless for <1 ppm (or no data available), light red for >1 ppm, and dark red for >2 ppm. Panel C was generated with MOLSCRIPT (*53*) and RASTER3D (*54*).

and the differences in the ^{15}N HSQC spectra can be attributed to the protonation of side chain carboxylate groups (*24*).

To our surprise, the ^{15}N HSQC spectrum of the same pH 4.0 sample of Sap-C dramatically changed when recorded again after several hours at 37 °C (Figure 5B). Although the original set of peaks is still visible with approximately 15% of its initial intensity, many new and much broader signals have emerged. The number of peaks and average ^{15}N relaxation rates are consistent with a homodimeric protein with a molecular correlation time (τ_c) of 10 ± 1 ns. Our attempts to reverse this transformation by dilution or storage of the sample at low temperatures were unsuccessful, and it also occurred in a dilute (0.2 mM) sample under the same conditions, albeit at a slower rate. This indicates that the new species is a specific dimer which seems to be the thermodynamically favored form of Sap-C at pH 4.0, whereas the monomeric form can be studied only at lower temperatures directly following gel filtration. Whereas below 27 °C the dimerization was too slow to compete with irreversible aggregation of the protein, it was usually complete within a few minutes at 57 °C.

At this temperature, the increased resolution enabled the assignment of most of the new ^{15}N HSQC peaks except for the N-terminal half of helix α1, whose resonances are still strongly overlapped. It turned out that the pattern arising from the hexahistidine tag remains completely unaffected (Figure 5); the tag is therefore not involved in the dimerization. The ^{15}N chemical shift changes between monomeric and dimeric Sap-C are plotted versus the residue number in Figure 6B and onto the structure of monomeric Sap-C in Figure 6C. The largest perturbations occur for residues in and close to the two spatially proximate loops, α1−α2 and α4−α5, suggesting they serve as either a dimer interface or a conformational hinge. Additionally, a strong shift and broadening of the signal belonging to the side chain NH_2 group of Asn^{21} (α1−α2 loop) indicates it loses flexibility and is now buried from the solvent.

DISCUSSION

Comparison of Sap-A, Sap-C, and Sap-D. Although the human saposins A−D are sequentially related with up to 40% identity, we found in this study remarkable differences in their behavior in solution. In contrast to Sap-C, whose structure has recently been determined using ^{13}C-labeled protein and traditional NMR methodology, Sap-A, Sap-B, and Sap-D are not conformationally homogeneous. Instead of full structure determinations of Sap-A and Sap-D, we therefore focused on a comparison of backbone NOE data and N−H^N residual dipolar couplings, which can be obtained relatively fast from ^{15}N-labeled proteins only. Assignment of ^{15}N HSQC spectra typically required 1 week of spectrometer time and 1 week for the analysis. The method used here is, of course, limited to small or helical proteins, since the sequential $d_{NN}(i, i + 1)$ correlations in β-sheets are often weak and difficult to distinguish from intermediate and long-range correlations.

The analogies of secondary structures, assigned ^{15}N HSQC spectra, and sequential patterns of N−H^N dipolar couplings provide evidence that at pH 7.0 both Sap-A and Sap-D adopt the monomeric "saposin" fold of Sap-C. Under these conditions, the saposins are highly negatively charged, which, together with the presence of three stabilizing disulfide bonds, explains their remarkable thermal robustness and the weak tendency to associate unspecifically. The results of fitting the measured dipolar couplings suggest that the structural variations among Sap-A, Sap-C, and Sap-D occur mainly in loop regions and helix α2 and are on the order of the variations between the determined structures of Sap-C and the homologue NK-lysin. In contrast to that in NK-lysin, helix α2 in Sap-C is curved with a more pronounced kink between Lys^{34} and Met^{35}, which is also present in Sap-A and Sap-D. The conformational exchange processes in Sap-A and Sap-D are associated with minor structural perturbations.

It has already been shown that ^{15}N HSQC spectra of Sap-C at pH 6.8 and 5.4 are virtually superimposable, and larger ^{15}N chemical shift perturbations upon further acidification to pH 4.2 occur mainly for titratable aspartate and glutamate residues (*24*). The authors concluded that Sap-C does not undergo a conformational change, and the pH dependence of Sap-C's membrane binding activity is sufficiently explained by charge neutralization of carboxylate groups. We confirmed this result down to pH 4.0, representing the

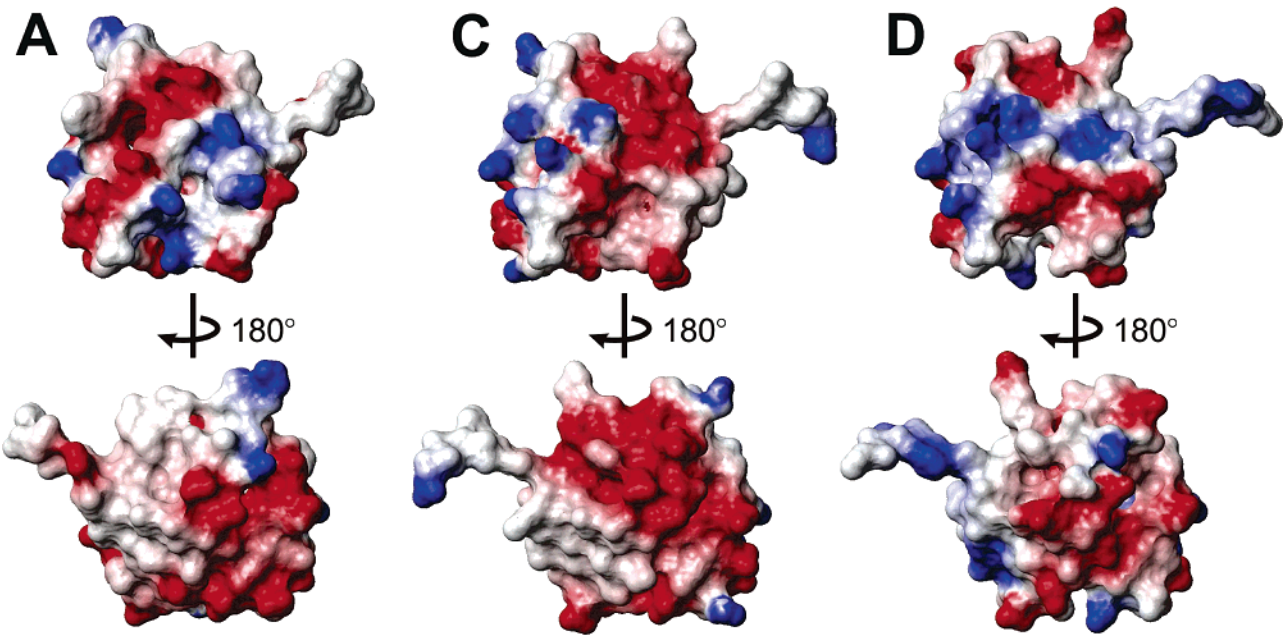

FIGURE 7: Front and back views of the surface electrostatic potential of Sap-A, Sap-C, and Sap-D at pH 7.0. Red and blue colors denote negatively (Asp and Glu) and positively (Arg, His, and Lys) charged residues, respectively, and the C-terminal residues after His^{82} (top right corners) were omitted. Sap-A and Sap-D are represented by protein models derived from Sap-C. This figure was generated with MOLMOL (*56*) using a standard macro for coloring.

minimum pH at which spectra could be recorded for a reasonable time period before irreversible aggregation of Sap-C occurred. ^{15}N HSQC spectra of Sap-D recorded at pH 4.0 indicate that the absence of a conformational change is likely to be also valid for this protein. Therefore, the specificity of Sap-A, Sap-C, and Sap-D for different lipids and hydrolases must originate from either the small structural differences between the molecules, a nonconservation of surface charges, or both. Figure 7 shows that, assuming similar structures, their surface electrostatic potentials are indeed remarkably different. For example, the lysine residues, which are responsible for Sap-C's fusogenetic activity (*55*), are located within the N-terminal half of the sequence, i.e., on the α1−α2 face, whereas in Sap-A, they are clustered in a region formed by helix α1 and the α4−α5 loop.

Unique Behavior of Sap-B. Biophysical data indicate that the in vivo role of Sap-B is quite different from that of the other saposins. It seems to act as a physiological detergent that forms nonspecific soluble complexes with sulfatide and other glycolipids rather than as an allosteric activator (*57*, *58*). The large hydrophobic cavity in the dimeric crystal structure of Sap-B (*25*) is likely to serve as a lipid binding pocket for this purpose. We have measured diffusion coefficients of Sap-B and Sap-C at pH 7.0 and found that also in solution Sap-B forms higher-order oligomeric associates, the data being consistent with a dimeric state. The broadening of resonances in the ^{15}N HSQC spectra may then be explained by the existence of millisecond conformational exchange within the dimer, as three different conformations have also been observed in the crystals (*25*).

The amino acid sequence of Sap-B (Figure 1) has a lower degree of similarity to those of the group of the other saposins (15−20% identical) and comprises a few distinct features, which may favor folding into a V-shaped dimer. First, the hydrophilic and hydrophobic positions of Asp^7 and Ile^9 (helix α1) are swapped, and the uniquely hydrophobic side chains of Ile^{46} (helix α3) from the two monomeric units face each other. Second, a major conformational difference between Sap-B and Sap-C occurs in the α1−α2 loop, where a phenylalanine is inserted (after Thr^{24}) and followed by another hydrophobic residue (Val^{25}). These two residues contribute to the interface and line the inner cavity of the dimeric structure. The most striking feature of the Sap-B structure, however, is the merging of α3 and α4 into a single long helix. In the other saposins, a sharp turn is introduced at this position by either of the "helix-breaking" residues (Gly^{55} and Pro^{56}). Finally, also the sequence motifs in the remaining α2−α3 and α4−α5 loop regions are characteristic of Sap-B.

Dimerization of Sap-C. In a recent study, it was shown that the ^{15}N HSQC spectrum of Sap-C at pH 6.8 dramatically changes in the presence of 7 molar equiv of the detergent SDS (*26*). A solution structure was determined, which showed that the compact saposin fold of five helices opens and adopts a tertiary structure similar to the V of crystalline Sap-B. Further results from ^{15}N relaxation and multiangle light scattering suggested that, at a protein concentration of 1 mM, the molecule is predominantly dimeric. However, the extent of self-association was reduced at lower protein concentrations, and the lack of intermolecular NOEs indicated that it is rather unspecific. Furthermore, the apparent molecular size was even larger when the pH was lowered to 5.4.

We observed a slow change of the pH 4.0 ^{15}N HSQC spectrum of Sap-C at elevated temperatures and found that the new peaks belong to a presumably dimeric species. As shown in Figure 6, the ^{15}N shift differences for monomeric and dimeric Sap-C at pH 4.0 correlate well with the shift differences induced by the presence of SDS, and a similar correlation can be found for H^N and H^α nuclei (data not shown). For both, the largest perturbations occur in the α1−α2 and α4−α5 loops, which serve as hinges for the opening of the Sap-C structure in a detergent environment. In contrast, we observed much smaller perturbations for the remaining

protein, particularly in the α3−α4 loop which represents another important hinge between the closed and open form of Sap-C. Furthermore, we noted that Asn^{21} becomes buried in the dimer, whereas residue 21 is solvent exposed in both Sap-C−SDS and Sap-B structures. Unfortunately, due to the limited sample stability, the quality of the NOESY-^{15}N HSQC spectrum was very poor and did not allow for a more detailed study of "our" dimer.

Any substantial opening of the saposin fold would lead to a number of hydrophobic side chains becoming solvent-exposed. In the presence of SDS, the resulting hydrophobic patches can bind the alkyl chains of the detergent molecules, which has been shown for Sap-C with the occurrence of intermolecular NOEs (*26*). However, in a purely aqueous solution, hydrophobic patches can be buried only if the protein forms specific oligomeric states, which occurs for the two clasping monomers of Sap-B (*25*). Likewise, we believe that the dimerization of Sap-C at acidic pH is highly specific as the resonance positions and line widths were reproducible in a dilute sample. Another clip-on model of two Sap-C molecules, each of which is anchored on opposing liposomal membranes, was proposed by Wang et al. to explain the fusogenetic activity of Sap-C (*18*). Using peptides mimicking the individual helices, it was shown that α1 and α5 are responsible for membrane binding, whereas α2 is involved in the protein−protein interaction. For the above-mentioned reason, this extremely open model is unlikely to exist in aqueous solution.

ACKNOWLEDGMENT

We are grateful to Natascha Remmel and Ralf Klingenstein for providing saposin expression vectors or transformed *P. pastoris* strains and to Maike Schoeniger for excellent technical assistance. We also thank Martin Tollinger for providing a MATLAB code for fitting exchange data and Jochen Klages for measuring RDCs of Sap-D.

REFERENCES

1. Furst, W., and Sandhoff, K. (1992) Activator proteins and topology of lysosomal sphingolipid catabolism, *Biochim. Biophys. Acta 1126*, 1−16.
2. Kishimoto, Y., Hiraiwa, M., and Obrien, J. S. (1992) Saposins: Structure, function, distribution, and molecular genetics, *J. Lipid Res. 33*, 1255−1267.
3. Vaccaro, A. M., Salvioli, R., Barca, A., Tatti, M., Ciaffoni, F., Maras, B., Siciliano, R., Zappacosta, F., Amoresano, A., and Pucci, P. (1995) Structural analysis of saposin C and saposin B: Complete localization of disulfide bridges, *J. Biol. Chem. 270*, 9953−9960.
4. Tatti, M., Salvioli, R., Ciaffoni, F., Pucci, P., Andolfo, A., Amoresano, A., and Vaccaro, A. M. (1999) Structural and membrane-binding properties of saposin D, *Eur. J. Biochem. 263*, 486−494.
5. Mehl, E., and Jatzkewitz, H. (1964) A cerebroside sulfatase from swine kidney, *Hoppe-Seyler's Z. Physiol. Chem. 339*, 260−276.
6. Linke, T., Wilkening, G., Lansmann, S., Moczall, H., Bartelsen, O., Weisgerber, J., and Sandhoff, K. (2001) Stimulation of acid sphingomyelinase activity by lysosomal lipids and sphingolipid activator proteins, *Biol. Chem. 382*, 283−290.
7. Matsuda, J., Kido, M., Tadano-Aritomi, K., Ishizuka, I., Tominaga, K., Toida, K., Takeda, E., Suzuki, K., and Kuroda, Y. (2004) Mutation in saposin D domain of sphingolipid activator protein gene causes urinary system defects and cerebellar Purkinje cell degeneration with accumulation of hydroxy fatty acid-containing ceramide in mouse, *Hum. Mol. Genet. 13*, 2709−2723.
8. Kolter, T., and Sandhoff, K. (1999) Sphingolipids: Their metabolic pathways and the pathobiochemistry of neurodegenerative diseases, *Angew. Chem., Int. Ed. 38*, 1532−1568.
9. Spiegel, R., Bach, G., Sury, V., Mengistu, G., Meidan, B., Shalev, S., Shneor, Y., Mandel, H., and Zeigler, M. (2005) A mutation in the saposin A coding region of the prosaposin gene in an infant presenting as Krabbe disease: First report of saposin A deficiency in humans, *Mol. Genet. Metab. 84*, 160−166.
10. Matsuda, J., Vanier, M. T., Saito, Y., Tohyama, J., Suzuki, K., and Suzuki, K. (2001) A mutation in the saposin A domain of the sphingolipid activator protein (prosaposin) gene results in a late-onset, chronic form of globoid cell leukodystrophy in the mouse, *Hum. Mol. Genet. 10*, 1191−1199.
11. Fujita, N., Suzuki, K., Vanier, M. T., Popko, B., Maeda, N., Klein, A., Henseler, M., Sandhoff, K., Nakayasu, H., and Suzuki, K. (1996) Targeted disruption of the mouse sphingolipid activator protein gene: A complex phenotype, including severe leukodystrophy and wide-spread storage of multiple sphingolipids, *Hum. Mol. Genet. 5*, 711−725.
12. Doering, T., Holleran, W. M., Potratz, A., Vielhaber, G., Elias, P. M., Suzuki, K., and Sandhoff, K. (1999) Sphingolipid activator proteins are required for epidermal permeability barrier formation, *J. Biol. Chem. 274*, 11038−11045.
13. Kang, S.-J., and Cresswell, P. (2004) Saposins facilitate CD1d-restricted presentation of an exogenous lipid antigen to T cells, *Nat. Immunol. 5*, 175−181.
14. Zhou, D. P., Cantu, C., Sagiv, Y., Schrantz, N., Kulkarni, A. B., Qi, X. Y., Mahuran, D. J., Morales, C. R., Grabowski, G. A., Benlagha, K., Savage, P., Bendelac, A., and Teyton, L. (2004) Editing of CD1d-bound lipid antigens by endosomal lipid transfer proteins, *Science 303*, 523−527.
15. Winau, F., Schwierzeck, V., Hurwitz, R., Remmel, N., Sieling, P. A., Modlin, R. L., Porcelli, S. A., Brinkmann, V., Sugita, M., Sandhoff, K., Kaufmann, S. H. E., and Schaible, U. E. (2004) Saposin C is required for lipid presentation by human CD1b, *Nat. Immunol. 5*, 344−344.
16. Ciaffoni, F., Salvioli, R., Tatti, M., Arancia, G., Crateri, P., and Vaccaro, A. M. (2001) Saposin D solubilizes anionic phospholipid-containing membranes, *J. Biol. Chem. 276*, 31583−31589.
17. Vaccaro, A. M., Tatti, M., Ciaffoni, F., Salvioli, R., Serafino, A., and Barca, A. (1994) Saposin C induces pH-dependent destabilization and fusion of phosphatidylserine-containing vesicles, *FEBS Lett. 349*, 181−186.
18. Wang, Y., Grabowski, G. A., and Qi, X. Y. (2003) Phospholipid vesicle fusion induced by saposin C, *Arch. Biochem. Biophys. 415*, 43−53.
19. You, H. X., Qi, X. Y., Grabowski, G. A., and Yu, L. (2003) Phospholipid membrane interactions of saposin C: In situ atomic force microscopic study, *Biophys. J. 84*, 2043−2057.
20. You, H. X., Qi, X. Y., and Yu, L. (2004) Direct AFM observation of saposin C-induced membrane domains in lipid bilayers: From simple to complex lipid mixtures, *Chem. Phys. Lipids 132*, 15−22.
21. Munford, R. S., Sheppard, P. O., and Ohara, P. J. (1995) Saposin-like proteins (SAPLIPs) carry out diverse functions on a common backbone structure, *J. Lipid Res. 36*, 1653−1663.
22. Kervinen, J., Tobin, G. J., Costa, J., Waugh, D. S., Wlodawer, A., and Zdanov, A. (1999) Crystal structure of plant aspartic proteinase prophytepsin: Inactivation and vacuolar targeting, *EMBO J. 18*, 3947−3955.
23. Liepinsh, E., Andersson, M., Ruysschaert, J. M., and Otting, G. (1997) Saposin fold revealed by the NMR structure of NK-lysin, *Nat. Struct. Biol. 4*, 793−795.
24. de Alba, E., Weiler, S., and Tjandra, N. (2003) Solution structure of human saposin C: pH-dependent interaction with phospholipid vesicles, *Biochemistry 42*, 14729−14740.
25. Ahn, V. E., Faull, K. F., Whitelegge, J. P., Fluharty, A. L., and Prive, G. G. (2003) Crystal structure of saposin B reveals a dimeric shell for lipid binding, *Proc. Natl. Acad. Sci. U.S.A. 100*, 38−43.
26. Hawkins, C. A., de Alba, E., and Tjandra, N. (2005) Solution structure of human saposin C in a detergent environment, *J. Mol. Biol. 346*, 1381−1392.
27. Vaccaro, A. M., Salvioli, R., Tatti, M., and Ciaffoni, F. (1999) Saposins and their interaction with lipids, *Neurochem. Res. 24*, 307−314.
28. Soeda, S., Hiraiwa, M., Obrien, J. S., and Kishimoto, Y. (1993) Binding of cerebrosides and sulfatides to saposins A−D, *J. Biol. Chem. 268*, 18519−18523.

29. Wendeler, M., Hoernschemeyer, J., John, M., Werth, N., Schoeniger, M., Lemm, T., Hartmann, R., Kessler, H., and Sandhoff, K. (2004) Expression of the GM2-activator protein in the methylotrophic yeast *Pichia pastoris*, purification, isotopic labeling, and biophysical characterization, *Protein Expression Purif. 34*, 147−157.
30. Hiraiwa, M., Soeda, S., Martin, B. M., Fluharty, A. L., Hirabayashi, Y., Obrien, J. S., and Kishimoto, Y. (1993) The effect of carbohydrate removal on stability and activity of saposin B, *Arch. Biochem. Biophys. 303*, 326−331.
31. Thompson, J. D., Gibson, T. J., Plewniak, F., Jeanmougin, F., and Higgins, D. G. (1997) The CLUSTAL_X windows interface: Flexible strategies for multiple sequence alignment aided by quality analysis tools, *Nucleic Acids Res. 25*, 4876−4882.
32. Laroche, Y., Storme, V., Demeutter, J., Messens, J., and Lauwereys, M. (1994) High-level secretion and very efficient isotopic labeling of tick anticoagulant peptide (TAP) expressed in the methylotrophic yeast, *Pichia pastoris*, *Nat. Biotechnol. 12*, 1119−1124.
33. Jerschow, A., and Muller, N. (1997) Suppression of convection artifacts in stimulated-echo diffusion experiments. Double-stimulated-echo experiments, *J. Magn. Reson. 125*, 372−375.
34. Jahnke, W., Baur, M., Gemmecker, G., and Kessler, H. (1995) Improved accuracy of NMR structures by a modified NOESY-HSQC experiment, *J. Magn. Reson., Ser. B 106*, 86−88.
35. Frenkiel, T., Bauer, C., Carr, M. D., Birdsall, B., and Feeney, J. (1990) HMQC-NOESY-HMQC, a 3-dimensional NMR experiment which allows detection of nuclear Overhauser effects between protons with overlapping signals, *J. Magn. Reson. 90*, 420−425.
36. Zhang, O. W., Kay, L. E., Olivier, J. P., and Formankay, J. D. (1994) Backbone H-1 and N-15 resonance assignments of the N-terminal SH3 domain of drk in folded and unfolded states using enhanced-sensitivity pulsed-field gradient NMR techniques, *J. Biomol. NMR 4*, 845−858.
37. Archer, S. J., Ikura, M., Torchia, D. A., and Bax, A. (1991) An alternative 3D-NMR technique for correlating backbone N-15 with side-chain H-β-resonances in larger proteins, *J. Magn. Reson. 95*, 636−641.
38. Briand, J., and Ernst, R. R. (1991) Computer-optimized homonuclear TOCSY experiments with suppression of cross relaxation, *Chem. Phys. Lett. 185*, 276−285.
39. Ottiger, M., Delaglio, F., and Bax, A. (1998) Measurement of J and dipolar couplings from simplified two-dimensional NMR spectra, *J. Magn. Reson. 131*, 373−378.
40. Schwede, T., Kopp, J., Guex, N., and Peitsch, M. C. (2003) SWISS-MODEL: An automated protein homology-modeling server, *Nucleic Acids Res. 31*, 3381−3385.
41. Dosset, P., Hus, J. C., Marion, D., and Blackledge, M. (2001) A novel interactive tool for rigid-body modeling of multi-domain macromolecules using residual dipolar couplings, *J. Biomol. NMR 20*, 223−231.
42. Farrow, N. A., Zhang, O. W., Formankay, J. D., and Kay, L. E. (1994) A heteronuclear correlation experiment for simultaneous determination of N-15 longitudinal decay and chemical-exchange rates of systems in slow equilibrium, *J. Biomol. NMR 4*, 727−734.
43. Tjandra, N., and Bax, A. (1997) Direct measurement of distances and angles in biomolecules by NMR in a dilute liquid crystalline medium, *Science 278*, 1111−1114.
44. Hansen, M. R., Mueller, L., and Pardi, A. (1998) Tunable alignment of macromolecules by filamentous phage yields dipolar coupling interactions, *Nat. Struct. Biol. 5*, 1065−1074.
45. Mesleh, M. F., Veglia, G., DeSilva, T. M., Marassi, F. M., and Opella, S. J. (2002) Dipolar waves as NMR maps of protein structure, *J. Am. Chem. Soc. 124*, 4206−4207.
46. Ojennus, D. D., Mitton-Fry, R. M., and Wuttke, D. S. (1999) Induced alignment and measurement of dipolar couplings of an SH2 domain through direct binding with filamentous phage, *J. Biomol. NMR 14*, 175−179.
47. Zweckstetter, M., Hummer, G., and Bax, A. (2004) Prediction of charge-induced molecular alignment of biomolecules dissolved in dilute liquid-crystalline phases, *Biophys. J. 86*, 3444−3460.
48. Dunitz, J. D. (1995) Win some, lose some: Enthalpy−entropy compensation in weak intermolecular interactions, *Chem. Biol. 2*, 709−712.
49. Cornish-Bowden, A. (2002) Enthalpy−entropy compensation: A phantom phenomenon, *J. Biosci. 27*, 121−126.
50. Kordel, J., Forsen, S., Drakenberg, T., and Chazin, W. J. (1990) The rate and structural consequences of proline cis−trans isomerization in calbindin-D9k: NMR-studies of the minor (cis-Pro43) isoform and the Pro43Gly mutant, *Biochemistry 29*, 4400−4409.
51. Otting, G., Liepinsh, E., and Wuthrich, K. (1993) Disulfide bond isomerization in BPTI and BPTI(G36S): An NMR-study of correlated mobility in proteins, *Biochemistry 32*, 3571−3582.
52. Kessler, H., and Rundel, W. (1968) Detection of internal molecular mobility by NMR spectroscopy. Conformation and hindered rotation in disulfides and diselenides, *Chem. Ber. 101*, 3350−3357.
53. Kraulis, P. J. (1991) MOLSCRIPT: A program to produce both detailed and schematic plots of protein structures, *J. Appl. Crystallogr. 24*, 946−950.
54. Merritt, E. A., and Murphy, M. E. P. (1994) RASTER3D version 2.0: A program for photorealistic molecular graphics, *Acta Crystallogr. D50*, 869−873.
55. Qi, X. Y., and Chu, Z. T. (2004) Fusogenic domain and lysines in saposin C, *Arch. Biochem. Biophys. 424*, 210−218.
56. Koradi, R., Billeter, M., and Wuthrich, K. (1996) MOLMOL: A program for display and analysis of macromolecular structures, *J. Mol. Graphics Modell. 14*, 51−55.
57. Fischer, G., and Jatzkewitz, H. (1977) Activator of cerebroside sulfatase: Binding studies with enzyme and substrate demonstrating detergent function of activator protein, *Biochim. Biophys. Acta 481*, 561−572.
58. Li, S. C., Sonnino, S., Tettamanti, G., and Li, Y. T. (1988) Characterization of a nonspecific activator protein for the enzymatic hydrolysis of glycolipids, *J. Biol. Chem. 263*, 6588−6591.

BI051944+